Design of Systematic GIRA Codes for CPM

Tarik Benaddi*†‡, Charly Poulliat†‡,
Marie-Laure Boucheret †‡, Benjamin Gadat§ and Guy Lesthievent*
*CNES-Toulouse †University of Toulouse, ENSEEIHT/IRIT
‡TéSA - Toulouse §Thales Alenia Space-Toulouse

***Abstract*—In this paper, we derive an asymptotic analysis for the design of serially concatenated turbo schemes that works for both systematic generalized irregular repeat accumulate (GIRA) and low density generator matrix (LDGM) codes concatenated with a continuous phase modulation (CPM). The proposed design is based on a semi-analytic EXIT chart optimization method. By considering a particular scheduling, inserting partial interleavers between GIRA accumulator and CPM and allowing degree-1 variable nodes, we show that one can achieve very good thresholds.**

I. Introduction

Continuous phase modulation (CPM) represents a subset of phase modulation family where the phase is kept continuous between signal intervals. The phase continuity and the constant envelope characteristics makes this family a very good choice to achieve excellent spectral efficiency and bit error rates in comparison to other phase modulations especially in nonlinear systems and channels. Because of these theoretical properties, this kind of modulation is considered with a big interest particularly since [1] rewrites the CPM modulator as a concatenation of a time-invariant continuous phase encoder (CPE) with a time-invariant memoryless modulator (MM).

Many studies have been conducted trying to jointly optimize iterative schemes with different CPM configurations and convolutional outer codes [2]–[4]. Later on, several code families emerged such as irregular repeat accumuluate (IRA) codes [5]. The main advantage of IRA codes is their low encoding and decoding complexity (linear in code length) while showing similar performance to low density parity check (LDPC) codes. Only few papers studied the convergence behaviour and the asymptotic design for general CPM schemes without relying on properties of some particular CPM families. [6]–[8] have considered an non systematic IRA-like coded CPM. The proposed structure replaces the IRA accumulator with a CPM modulator. This was motivated by the fact that CPM acts as a phase accumulator. Recently, [9] has investigated the design of both unstructured LDPC and protograph codes. All these methods, when applied to systematic general IRA codes, are not straightforward.

The main contribution of this paper is to propose a general framework to represent, analyse and design any generalized systematic IRA code (GIRA) serially concatenated with any CPM scheme. In GIRA codes, the accumulator $1/(1+D)$ is replaced with a generalized accumulator with a polynomial transfer function $1/G(D)$. Not only this class offers more flexibility but also embraces all previously discussed codes by choosing the right accumulator function. Furthermore, we point out that for systematic GIRA codes, the optimization is not as straightforward as the non systematic case [6], [10] but requires a well-thought scheduling. Also, we have not to consider, at the difference of [6], [11], to carefully design doping check nodes [12]. Additionally, we can remark that the extrinsic information transfer function (EXIT) [13] of CPM detectors, at the difference of the MIMO detector in [11], joins the point $(1,1)$. Consequently, we are allowed to introduce degree-1 variable nodes.

The paper is organized as follows: Section II describes the general model of serially concatenated GIRA-CPM systems. Section III provides the convergence analysis based on asymptotic EXIT analysis. Finally, Section IV presents some design and performance examples.

II. System Description

A systematic GIRA code serially concatenated with a CPM modulator is depicted in Fig. 1a. GIRA encoder can be seen as a serial concatenation of repetition codes with a convolutional code named accumulator. In non systematic GIRA codes, the information bits are not transmitted. At the beginning of the coding process, each bit of a binary message $u \in \{0,1\}^K$ is irregularly repeated with a factor corresponding to the node degree of its associated variable node. After interleaving by a random interleaver π_{GIRA}, the repeated bits are first combined (using the so-called combiner) and then are fed to the "generalized" accumulator, with polynomial transfer function $1/G(D)$. The parity check matrix of a systematic GIRA code is of the form $H = [H_u H_p]$ where H_u refers to the connections between the systematic bits variable nodes and the check nodes while the squared matrix H_p describes the connections between check nodes and parity bit variable nodes. To name only a few, when $G(D)=1$, we obtain a LDGM code, or again when $G(D)=1+D$ we have an IRA code. As for irregular LDPC, the sub-matrix H_u of GIRA codes ensemble can be represented with its edge-perspective degree distribution polynomials:

$$\lambda(x) = \sum_{i=1}^{d_v} \lambda_i x^{i-1} \quad , \quad \rho(x) = \sum_{j=1}^{d_c} \rho_j x^{j-1}$$

where λ_i (resp. ρ_j) is the proportion of edges in the Tanner graph connected to variable nodes (VN) of degree i (resp. to check nodes (CN) of degree j) and d_v (reps. d_c) is the maximum VN (resp. CN) degree. When the GIRA code is systematic and check-regular, the design code rate is given by:

$$R = \frac{d_c \sum \lambda_i / i}{1 + d_c \sum \lambda_i / i} \tag{1}$$

Each code word $\boldsymbol{c}$ is then interleaved, mapped into M-ary symbols $\boldsymbol{\alpha} = \{\alpha_i\}_i$ and finally encoded by the CPM:

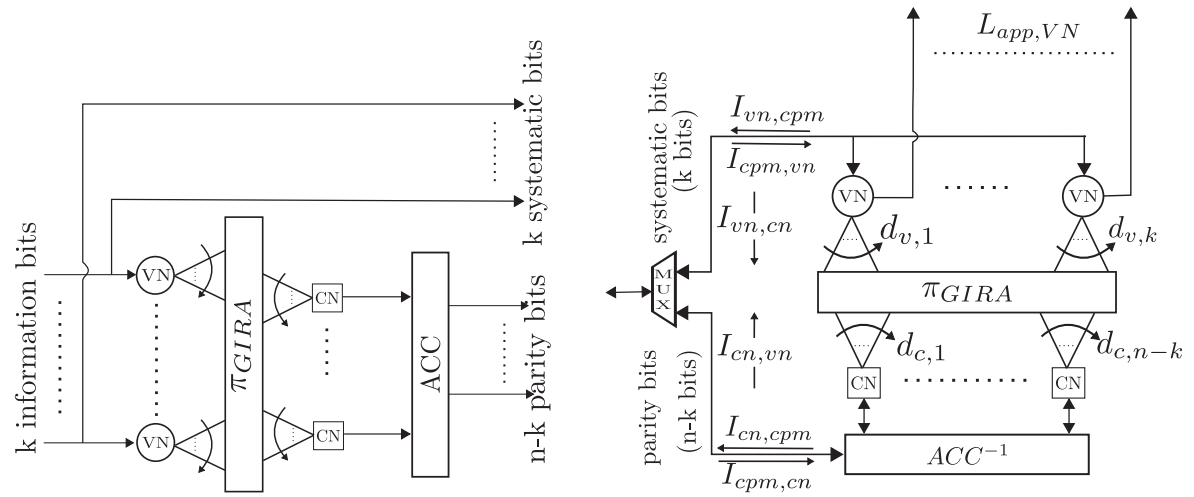

(a) GIRA encoder (b) Systematic GIRA soft decoder

Fig. 1: GIRA encoder and decoder

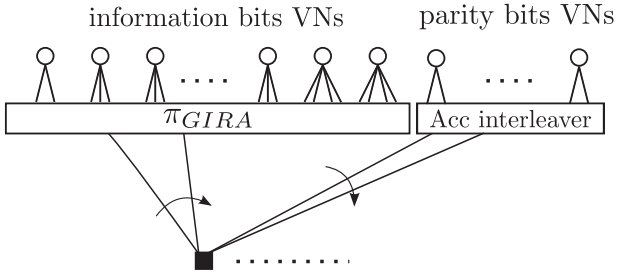

Fig. 2: GIRA Tanner graph

$$s(t,\boldsymbol{\alpha}) = \sqrt{\frac{2E_s}{T}} cos\left(2\pi f_0 t + \theta(t,\boldsymbol{\alpha}) + \theta_0\right) \quad (2)$$

with

$$\theta(t,\boldsymbol{\alpha}) = \pi h \sum_{i=0}^{N-1} \alpha_i q(t-iT), \quad q(t) = \begin{cases} \int_0^t g(\tau)d\tau \\ 1/2, \ t > L \end{cases}$$

f_0 is the carrier frequency, θ_0 the initial phase shift, $\theta(t,\boldsymbol{\alpha})$ the information carrying phase, $g(t)$ the frequency pulse, $h = k/p$ the modulation index, L the memory and $\Re$ the real part. Practically, the shape of $q(t)$ (rectangular (REC), raised-cosine (RC), ...) and L determine the smoothness of the signal.

At the receiver side, the soft-input soft-output (SISO) CPM decoder is based on the Rimoldi decomposition [1] which splits the CPM modulator into a serial concatenation of the CPE, represented by a trellis, and the MM, seen as a filter bank. The information symbols $\boldsymbol{\alpha}$ are taken in $\{\pm 1, ..., \pm(M-1)\}$ whatever the parity of M is and figure in the tilted phase as:

$$\overline{\psi}(\tau + nT, \boldsymbol{\alpha}) = \left[\left[2\pi h \sum_{i=0}^{n-L} \alpha_i \right] \ mod\ p + W(\tau) \right.$$
$$\left. + 4\pi h \sum_{i=0}^{L-1} \alpha_{n-i} q(\tau + iT) \right] \ mod\ 2\pi \ , \ 0 \le \tau \le T$$

where $W(\tau)$ is a data independent term [1]. Rimoldi decomposition generates a trellis of pM^{L-1} states defined by the tuple $\sigma_n = [U_{n-1}, ..., U_{n-L+1}, V_n]$ where $V_n = [\sum_{i=0}^{n-L} U_i] mod\ p$. The MM is formed by pM^L different pulses $\{s_i(t)\}_i$ corresponding to CPE output symbols $X_n = [U_n, ..., U_{n-L+1}, V_n]$, where U_i is a M-ary modified data digit [1]. The transmitted signal $s(t,\boldsymbol{\alpha})$ is corrupted with an additive white Gaussian noise (AWGN) having a double-sided power spectral density $N_0/2$. From Eq. (2), the complex baseband noised signal can be written as follows:

$$y(t) = \sqrt{2E_s/T} exp\{j\psi(t,\boldsymbol{\alpha}\} + n(t) \ , \ t > 0 \quad (3)$$

The outputs of receiver matched filters bank $\{s^*(T-t)\}$ are sampled once each nT to obtain the correlator output $\boldsymbol{y^n} = [y_i^n = \int_{nT}^{(n+1)T} y(l) s_i^*(l) dl]_{1 \le i \le pM^L}$. It is shown that $\{\boldsymbol{y^n}\}_n$ are sufficient statistics to estimate symbols. Furthermore, using any orthonormal expansion of receiver matched filters bank [2], the joint probability density function of $\boldsymbol{y^n}$ can be reduced to $p(\boldsymbol{y^n}/X_n) \propto exp\{2Re(y_i^n)/N_0\}$. This measure can be used to compute transition metrics of the CPE trellis exploiting the BCJR algorithm [14]. For the outer decoder, we can use either LDPC-like decoding exploiting the belief-propagation (BP) algorithm [15] on the Tanner graph associated to GIRA code (see Fig. 2) or turbo-like decoding expanding the GIRA code into a serial concatenation of an LDGM and an accumulator [10]. Actually, these two methods are equivalent when the GIRA parity check matrix H is cycle free. Figure 1b depicts GIRA soft decoder architecture.

III. Code design

Density evolution algorithms to study the asymptotic convergence behavior of concatenated system can be cumbersome, instead, EXIT charts [16] are exploited. In AWGN, it is generally assumed that the probability density functions of exchanged log likelihood ratios (LLRs) can be well modeled with a consistent Gaussian distribution. As a result, we can evaluate the asymptotic evolution of different modules of the receiver by tracking only the variance σ^2 of their exchanged LLRs [16] using the function $J(\sigma) = 1 - E_x(log_2(1 + e^{-x}))$ with $x \sim N(\sigma^2/2, \sigma^2)$. Partially inspired from [6], our optimization method returns the best degree profiles using EXIT curve-fitting. In our case, since we have an accumulator and a systematic

encoder, we need to define a particular scheduling to obtain linear equations with respect to $\{\lambda_i\}$: the CPM decoder communicates its extrinsic LLR values to all variable nodes. Systematic variable nodes perform a data-pass operation to the check nodes that in turn forward their information to the accumulator. At this point, we can consider a subsystem formed by a serially concatenated convolution codes: the accumulator and the CPE. After a certain number of turbo-iterations, that will be characterized later, the accumulator propagates its extrinsic information back to the systematic variable nodes. This defines one global iteration ℓ. GIRA codes generalize IRA codes in that the accumulator $1/1+D$ is replaced by any convolutional code with transfer function $1/G(D)$ where $G(D) = 1+\sum_{i=1}^{i=r} g_i D^i$ with $g_i \in \{0,1\}$. In this paper, we will consider tail-bited GIRA codes. When choosing the accumulator, we must insure that the girth of H_p is greater than 4, for instance, $G(D) = 1 + D + D^2$ is not allowed. Furthermore, we will consider systematic GIRA codes so that there is no need to consider introducing doping check nodes [12].

Designing a GIRA code consists in picking out variable nodes profile $\lambda(x)$ and check nodes profile $\rho(x)$ that maximize the design rate for a given signal to noise ratio (SNR) E_s/N_0 with respect to the convergence of the decoding trajectories. Fig. 1b introduces the main notations of different mutual information associated with LLR messages and corresponding coded bits involved in the design. Basically, in our modelling, the set of edges connecting check nodes to parity variable nodes in Fig. 2 is not included neither in $\lambda(x)$ nor in $\rho(x)$. These connections, directly linked to the type of the accumulator, are taken into account in the EXIT transfer function as it is going to be explained later on. Besides, partial interleavers one per each VN degree between CPM and the systematic part of IRA are considered, the reason will be clarified in the following.

A. CPM transfer function

Assume $I_{.,cpm}$ and $I_{cpm,.}$ denote respectively the apriori and extrinsic mutual information of the CPM soft decoder. Analytical study of the input-output EXIT transfer function of SISO CPM module is not straightforward. Alternatively, we compute the CPM transfer chart $T_{cpm,\sigma_{noise}}$ using Monte Carlo simulation and polynomial approximation. Thus, we have:

$$I_{cpm,.} = T_{cpm,\sigma_{noise}}(I_{.,cpm}) \tag{4}$$

As we will consider a curve fitting approach and based on the commonly observed generalization of the results of [13] for the binary erasure channel, an upper bound on the achievable rate for the outer code given an SNR E_s/N_0 can be approximately using the area under the CPM detector EXIT curve, i.e.: $R \leq R^* = \int_0^1 T_{cpm,\sigma_{noise}}(I_{vn-cpm}) dI_{vn-cpm}$. Unlike MIMO receiver in [11], CPM detector EXIT curves join the point $(1,1)$: it allows us to introduce degree-1 VNs. Also, it will be implicitly assumed that BCJR recursions are run independently between different trellis section groups delimited by each partial interleaver. This is not the case in practice but this assumption allows us to neglect transition effects when running BCJR decoding. Marker-free line in Fig. 3 presents EXIT chart of GSM GMSK with $L = 3$, $h = 1/2$ and $BT = 0.3$ at $E_s/N_0 = 0$dB.

B. IRA transfer functions

1) EXIT Transfer Function of VNs and CNs: Let $I^{\ell}_{vn,cn}$ denotes the averaged mixture of extrinsic MI output from a variable node to check node at the ℓ^{th} iteration. The mixture of MIs sent from VNs to CNs is then equal to:

$$I^{\ell}_{vn,cn} = \sum_{i=1}^{d_v} \lambda_i I^{\ell}_{vn,cn}(i) \tag{5}$$

where $I^{\ell}_{vn-cn}(i)$ is the expected mutual information associated with LLRs passed from a VN of degree i to CNs and is given by:

$$I^{\ell}_{vn,cn}(i) = J\left(\sqrt{(i-1)[J^{-1}(I^{\ell-1}_{cn,vn}(i))]^2 + [J^{-1}(I^{\ell}_{cpm,vn}(i))]^2}\right) \tag{6}$$

Likewise, VN to CPM direction update function is given by:

$$I^{\ell-1}_{vn,cpm}(j) = J(\sqrt{i} J^{-1}(I^{\ell-1}_{cn,vn})) \tag{7}$$

Since the VN profile is not regular, assuming Eq. (7) is equivalent to considering partial interleavers per VN degree between CPM and the systematic part of GIRA. The idea behind this choice is in essence equivalent to [10] to enable linear programming optimization. Nevertheless, if one uses one global interleaver between CPM and GIRA, we are not allowed to write Eq. (7) but instead:

$$I^{\ell-1}_{vn,cpm} = \sum_{i=1}^{d_v} \tilde{\lambda}_i J(\sqrt{i} J^{-1}(I^{\ell-1}_{cn,vn}))$$

where $\tilde{\lambda}_i$ is the proportion of VN of degree i. When injecting this expression into Eq. (6), this assumption leads necessarily to nonlinear convergence constraints [1].

On the other hand, the information passed from CN of degree j to the parity bits nodes and to systematic variable nodes are respectively:

$$I^{\ell-1}_{cn,acc}(j) = 1 - J(\sqrt{j} J^{-1}\big(1 - I^{\ell-1}_{vn,cn}\big)) \tag{8}$$

$$I^{\ell-1}_{cn,vn}(j) = 1 - J\left(\sqrt{(j-1) J^{-1}\big(1 - I^{\ell-1}_{vn,cn}\big) + J^{-1}\big(1 - I^{\ell-1}_{acc,cn}\big)}\right) \tag{9}$$

Without loss of generality, we can suppose check-regular GIRA with uniform check degree d_c.

2) EXIT Transfer Function of Accumulator: [11] approximates $I^{\ell}_{acc,cn}$ by $\left[\frac{1-q}{1-qI^{\ell}_{cn,acc}}\right]^2$, $\quad q = 1 - \overline{I^{\ell}}_{cpm,acc}$ where $\overline{I^{\ell}}_{cpm,acc}$ corresponds to the convergence threshold between CPM seen as inner code and the accumulator seen as outer code. However, this expression is correct only for $G(D) = 1 + D$ and $d_c = 1$ [5]. In the general case, we shall precompute the different EXIT charts of

[1] Note that Eq. 8 in [17] is not consistent with the authors' proposed framework.

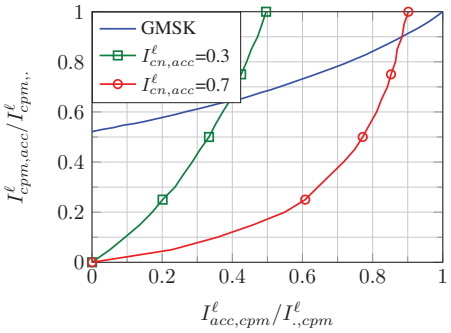

(a) IRA

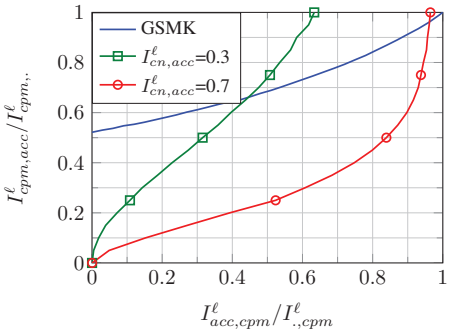

(b) GIRA with $G(D) = 1 + D + D^4$

Fig. 3: $I^{\ell}_{acc,cpm}$ as a function of $I^{\ell}_{cpm,acc}$ with different aprioris $I^{\ell}_{cn,acc}$ at $E_s/N_0 = 0$dB.

the accumulator ($I^{\ell}_{acc,cn}$ and $I^{\ell}_{acc,cpm}$) using Monte Carlo approximations:

$$I^{\ell}_{acc,cn} = T_{acc,cn}(\overline{I^{\ell}}_{cpm,acc}, I^{\ell}_{cn,acc}) \quad (10)$$

$$I^{\ell}_{acc,cpm} = T_{acc,cpm}(I^{\ell}_{acc,cn}, I^{\ell}_{cpm,acc}) \quad (11)$$

The former is the MI over uncoded bits whereas the latter is the MI over encoded bits.

Figures 3a and 3b illustrate the location of the convergence (intersection points) of the concatenated subsystem CPM+ACC. The unmarked curves correspond to the CPM (here a GMSK). The marked curves represent EXIT transfer functions of different accumulators as function of different apriori values. Figure 4 shows how $\overline{I^{\ell}}_{cpm,acc}$ varies as function of the apriori mutual information $I_{cn,acc}$. One can clearly observe that the convergence threshold is significantly improved if $I_{cn,acc}$ is relatively decided. The threshold of the system {accumulator, CPM} for a particular SNR can be easily provided by a curve-approximating polynomial of the curves depicted in Fig. 4. Even if GIRA codes present a small degradation of the decoding threshold in comparison to IRA codes [18], observe that the EXIT chart of former is better than the latter. Finally, we point out that for the special case of a LDGM code, there is no accumulator, i.e. $G(D) = 1$, therefore, $I^{\ell}_{acc,cn}$ and $I^{\ell}_{acc,cpm}$ are equal to $I^{\ell}_{cpm,acc}$ and $I^{\ell}_{cn,acc}$ respectively.

From Eqs. (7) to (11) we can compute the transfer function of joint CN and ACC+CPM. When combined with Eqs. (4) to (6), this leads to a linear programming problem that maximizes of the design rate R in Eq. (1) under the convergence constraints $\Phi(\boldsymbol{\lambda}, I^{(l)}_{vn,cn}, \sigma^2) = I^{(l+1)}_{vn,cn} > I^{(l)}_{vn,cn}, \forall I^{(l)}_{vn,cn} \in [0,1]$. By convention, $I^{(0)}_{vn,cpm}(i) = 0, \forall i = 1, ..., d_v$ and $I^{(0)}_{cn,vn} = 0$.

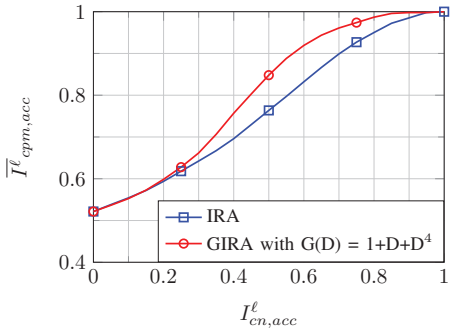

Fig. 4: Accumulator and GMSK convergence point (intersection) at $E_s/N_0 = 0$dB as function of $I_{cn,acc}$

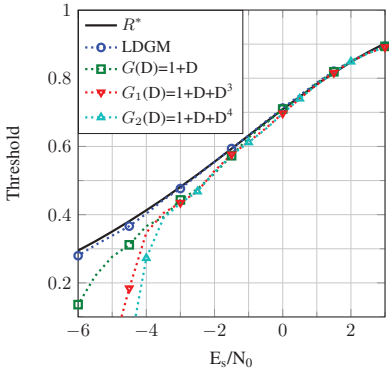

Fig. 5: Achievable and optimized rates when VNs degrees are constrained to be ≥ 1

GMSK: Threshold -2.73dB			
LDGM		IRA	
Threshold -2.7dB		Threshold -2.22dB	
$\lambda_1 = 0.051$ $\lambda_2 = 0.357$ $\lambda_5 = 0.023$ $\lambda_6 = 0.568$	$d_c = 3$	$\lambda_1 = 0.185$ $\lambda_2 = 0.551$ $\lambda_8 = 0.086$ $\lambda_9 = 0.176$	$d_c = 2$
G(D)=$1 + D + D^3$		G(D)=$1 + D + D^4$	
Threshold -2.22dB		Threshold -2.22dB	
$\lambda_1 = 0.411$ $\lambda_7 = 0.103$ $\lambda_8 = 0.485$	$d_c = 2$	$\lambda_1 = 0.424$ $\lambda_2 = 0.04$ $\lambda_{10} = 0.536$	$d_c = 2$

TABLE I: Optimized GIRA codes for design rate $R \simeq 0.5$. For LDPC code, we obtain $\lambda_1 = 0.1125, \lambda_2 = 0.5294, \lambda_5 = 0.0086, \lambda_{10} = 0.3495, \rho_3 = 0.2, \rho_4 = 0.8$ with a threshold of -2.7dB

IV. Simulation Results

In this section, we present some simulation results obtained from our optimization for four different GIRA codes: LDGM, IRA, $G_1(D) = 1 + D + D^3$ and $G_2(D) = 1 + D + D^4$. Figure 5 depicts obtained thresholds and compares them to the maximum achievable rate R^* for GSM GMSK. We observe that we operate very close to R^*. These results can be improved by allowing higher d_v (here $d_v = 10$). Table I presents some optimized profiles and their corresponding asymptotic thresholds. Note that the profile coefficients λ_i and d_c refer to H_u.

For comparison, taking the case of the memory-1 Minimum Shift Keying (MSK) CPM, the threshold for designed nonsystematic rate-1/2 LDGM in [6] is $E_s/N_0 = -2.61$dB, while our optimization gives a systematic rate-1/2 LDGM code with threshold -2.7dB (values are to be compared with the MSK theoretical threshold -2.8dB). Figure 6 illustrates how the designed rates depend on the minimum degree of VNs $d_{v,min}$. While introducing degree-1 VNs leads to a slight improvement in the case

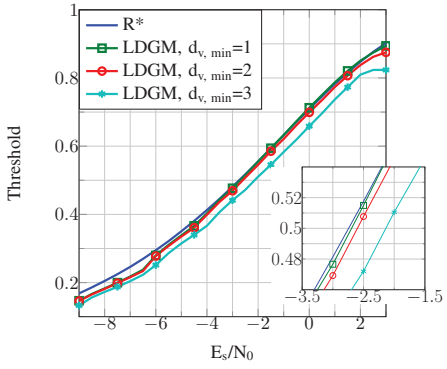

(a) LDGM

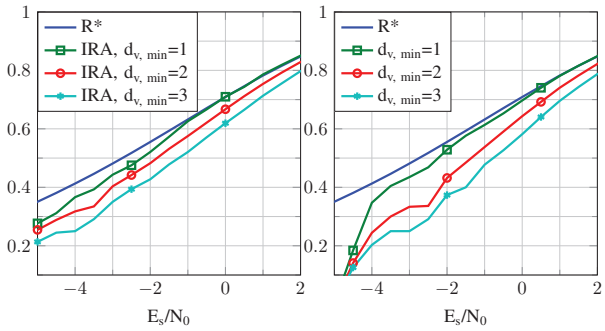

(b) IRA (c) $G(D) = 1 + D + D^4$

Fig. 6: Maximum achievable and optimized rates for some GIRA codes with GMSK

of LDGM, in the case of IRA, GIRA $G_1(D)$ and GIRA $G_2(D)$, it outperforms clearly $d_{v,min} = 2$ schemes by a gain of 0.4 dB, 0.9 dB and 0.92 dB respectively at rate of 0.5. Finally, Fig. 7 plots bit error rate (BER) as function of E_s/N_0 for different optimized GIRA profiles in Table I. We used around 16000 information bits with 200 CPM-GIRA turbo iterations, the construction of the matrix H is random. As expected, IRA presents a small gain in the threshold region in comparison to the GIRA code corresponding to the generator polynomial $G_2(D)$. The floor of this latter arrives earlier in our study because of the introduction of degree-1 variable nodes and the random generation of H. For LDGM with $d_{v,min} = 1$, we have observed that the error floor region is generally higher for GMSK than [6] for MSK. This is mainly due to the high proportion of degree-1 VNs and the random generation of H. Results could be improved with a more structured design of the matrix H at finite length. Instead, for LDGM only, we will constrain $d_{v,min} \geq 2$. The used profile, always for H_u, is then $\lambda_2 = 0.367, \lambda_{10} = 0.633, d_c = 4$. This has only a minor impact on the theoretical threshold (cf. Fig. 6a).

V. Conclusion

We introduced a general framework for the asymptotic analysis and design of systematic GIRA codes serial concatenated with CPM. Among all families, it appears from the obtained results that IRA and LDGM codes present the best trade-off threshold performance. Future works will investigate the finite length design of GIRA codes family.

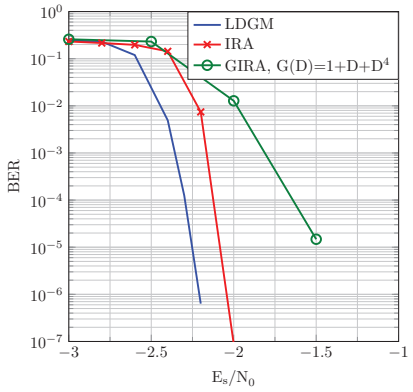

Fig. 7: Obtained BER of GIRA codes with GMSK

References

[1] B E Rimoldi, "A decomposition approach to cpm," *IEEE Trans. Inf. Theory*, vol. 34, no. 2, pp. 260–270, 1988.

[2] P Moqvist and T M Aulin, "Serially concatenated continuous phase modulation with iterative decoding," *IEEE Trans. Commun.*, vol. 49, no. 11, pp. 1901–1915, 2001.

[3] K R Narayanan and G L Stuber, "A serial concatenation approach to iterative demodulation and decoding," *IEEE Trans. Commun.*, vol. 47, no. 7, pp. 956–961, 1999.

[4] A Barbieri, D Fertonani, and G Colavolpe, "Spectrally-efficient continuous phase modulations," *IEEE Trans. Wireless Commun*, vol. 8, no. 3, pp. 1564–1572, 2009.

[5] H Jin, *Analysis and design of turbo-like codes*, Ph.D. thesis, California Institute of Technology, 2001.

[6] M Xiao and T Aulin, "Irregular repeat continuous phase modulation," *IEEE Commun. Lett*, vol. 9, no. 8, pp. 723–725, 2005.

[7] S Cheng, M C Valenti, and D Torrieri, "Coherent continuous-phase frequency-shift keying: parameter optimization and code design," *IEEE Trans. Wireless Commun.*, vol. 8, no. 4, pp. 1792–1802, 2009.

[8] M Xiao and Tor M Aulin, "On analysis and design of low density generator matrix codes for continuous phase modulation," *IEEE Trans. Wireless Commun.*, vol. 6, no. 9, pp. 3440–3449, 2007.

[9] T Benaddi, C Poulliat, ML Boucheret, ML Gadat, and G Lestievent, "Design of unstructured and protograph-based ldpc coded continuous phase modulation," *IEEE International Symposium of Information Theory. ISIT*, 2014.

[10] L Schmalen, S ten Brink, G Lechner, and A Leven, "On threshold prediction of low-density parity-check codes with structure," in *46th Annual Conference on Information Sciences and Systems (CISS), 2012*. IEEE, 2012, pp. 1–5.

[11] S ten Brink and G Kramer, "Design of repeat-accumulate codes for iterative detection and decoding," *IEEE Trans. Signal Process*, vol. 51, no. 11, pp. 2764–2772, 2003.

[12] S. ten Brink, "Code doping for triggering iterative decoding convergence," pp. 235–, 2001.

[13] A Ashikhmin, G Kramer, and S ten Brink, "Extrinsic information transfer functions: model and erasure channel properties," *IEEE Trans. Inf. Theory*, vol. 50, no. 11, pp. 2657–2673, 2004.

[14] L Bahl, J Cocke, F Jelinek, and J Raviv, "Optimal decoding of linear codes for minimizing symbol error rate (corresp.)," *IEEE Trans. Inf. Theory*, vol. 20, no. 2, pp. 284–287, 1974.

[15] T J Richardson and R L Urbanke, "The capacity of low-density parity-check codes under message-passing decoding," *IEEE Trans. Inf. Theory*, vol. 47, no. 2, pp. 599–618, 2001.

[16] S ten Brink, "Convergence behavior of iteratively decoded parallel concatenated codes," *IEEE Trans. Commun.*, vol. 49, no. 10, pp. 1727–1737, 2001.

[17] Zhang Nan, Gao Xiao, and Xu Ye-mao, "Jointly iterative decoding of low-density parity check codes (ldpc) coded continues phase modulation (cpm)," *Multidisciplinary Journals in Science and Technology. JSAT*, vol. 2, no. 3, pp. 25–31, 2011.

[18] S J Johnson and S R Weller, "Combinatorial interleavers for systematic regular repeat-accumulate codes [transactions letters]," *IEEE Trans. Commun*, vol. 56, no. 8, pp. 1201–1206, 2008.